

## Optimization and preliminary design of a high-temperature, low pressure-ratio sCO<sub>2</sub>-compressor for a wide operating range

Sebastian Rath\*  
Institute of Power Engineering  
TU Dresden  
Dresden, Germany

Sebastian Unger  
Institute of Fluid Dynamics  
Helmholtz-Zentrum Dresden-Rossendorf  
Dresden, Germany

Uwe Hampel  
Institute of Fluid Dynamics  
Helmholtz-Zentrum Dresden-Rossendorf  
Dresden, Germany

Uwe Gampe  
Institute of Power Engineering  
TU Dresden  
Dresden, Germany

### ABSTRACT

Power cycles based on supercritical carbon dioxide (sCO<sub>2</sub>) promise higher thermal efficiencies and more compact components than conventional technologies. Within the CARBOSOLA project, funded by the German Federal Ministry for Economic Affairs and Energy, a large-scale experimental facility is being set up by a consortium of scientific and industrial partners to actively contribute to the development of sCO<sub>2</sub> technology. The first expansion stage provides a circulation of the sCO<sub>2</sub> flow without expansion devices in the test loop. Thereby the compressor is intended to compensate for pressure losses and consequently for low pressure differences. In addition to that, a preferably wide operating range, regarding temperature and pressure, shall provide a high degree of flexibility of the test rig.

This work presents the design optimization of the impeller aiming at a wide operating range in compliance with the boundary conditions set for the test rig and the use of sCO<sub>2</sub>. For this purpose, a hybrid approach is used, combining parametric three-dimensional modeling with a one-dimensional performance criterion for operating range estimation. A large number of impeller designs have been simulated numerically within an optimization procedure using a genetic algorithm. On this basis, several designs have been selected and compared against each other. The evaluation includes sets of performance lines and the validation of the one-dimensional criterion used for optimization.

### INTRODUCTION

Looking for future-proof technologies for more efficient conversion of heat into electricity, power cycles based on sCO<sub>2</sub> represent a promising alternative to the conventional use of water based steam. A wide parameter range, higher efficiencies, and more compact components are expected to result in a more flexible and efficient usage of different heat sources from conventional and regenerative origin. However, additional research is needed to bring the technology to commercial maturity. Within the CARBOSOLA project (supercritical carbon dioxide as alternative working fluid for bottoming cycle and solar thermal application), funded by the German Federal Ministry for Economic Affairs and Energy, a large scale experimental facility is being set up by a consortium

\*Corresponding author, sebastian.rath@tu-dresden.de

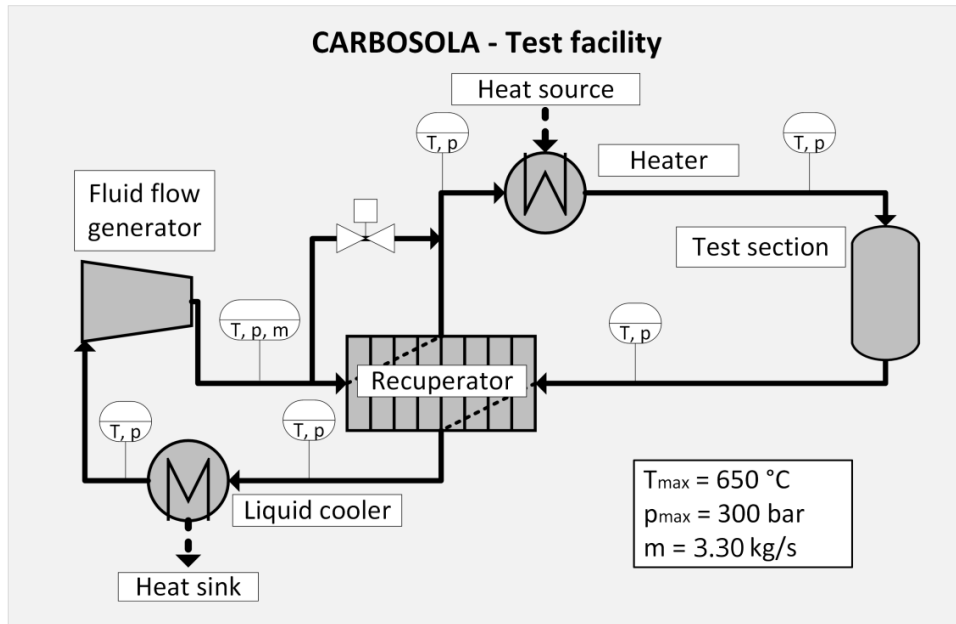


Figure 1: Block diagram and operating parameters of the first expansion stage of the CARBOSOLA test facility.

of scientific and industrial partners to actively contribute to the development of sCO<sub>2</sub> technology. Addressed topics range from basic research to large scale component testing. For the test rig a modular concept was chosen to easily enable future extensions in additional stages. As shown in Figure 1, the first expansion stage, which will be erected within the project, consists of a simple closed loop setup with fluid parameters up to 300 bar and 650 °C. As in this first stage no expansion device is planned, fluid circulation is provided by a compressor with a low pressure ratio to compensate occurring pressure losses in the system. A preferably wide operating range should be able to cover a wide variety of test scenarios. Nevertheless, a simple and “hassle-free” design should be preserved. To fit these requirements, a basic design is to be created and optimized within a numerical optimization procedure.

Since a preferable wide operating range is not only related to sCO<sub>2</sub> applications, several studies can be found addressing this topic. To give a few examples Ibaraki et al. [1] used an artificial neural network, combined with an genetic algorithm to improve the operating range of automotive turbochargers. Geometry modification was done using a total of 27 design variables defining the meridional contour as well as the configuration and shape of the blades. Range improvements could be shown for two optimized geometries. By targeting efficiency and range improvements Yagi et al. [2] studied the optimization of the blade loading distribution of centrifugal impellers. Using two different 3D design approaches large range improvements could be achieved compared to comparative impellers.

Pelton et al. [3] did a numerical study on the design of a wide range centrifugal impeller to be used as the first stage of a compressor for a 10 MWe sCO<sub>2</sub> power cycle application. As a first step various concepts for range extension were collected from the literature and ranked in terms of their potential and feasibility. Subsequently the best rated concepts were evaluated numerically by comparing against a baseline design. This showed that vaneless diffusers, splitter blades and casing treatments, allowing a passive shroud bleed, giving the largest effect regarding to a large operating range. On this base, by combining multiple concepts, a semi-shrouded impeller-casing configuration was created and further evaluated.

## DESIGN VARIABLES AND NUMERICAL SETUP

Oriented on the boundary conditions of the test rig, a baseline model was created to serve as a geometrical base for optimization. This was done using the commercial design software CFTurbo, which provides an integrated workflow for sizing, modeling and export to various CFD input formats. The meanline sizing values and initial performance estimates can be found in Table 1. Referring to the rig specification a mass flow rate of  $\dot{m} = 3.30 \text{ kg/s}$  was set. For the pressure difference an estimated value of  $\Delta p_{\text{tot}} = 10 \text{ bar}$  was selected to provide sufficient reserves compensating additional pressure losses caused by future experimental setups in the test section (cf. Figure 1). Based on the targeted operating pressure of 300 bar, this results in an inlet pressure of 290 bar and thus in a pressure ratio of  $\Pi_{\text{tot}} \approx 1.035$ . Regarding the inlet temperatures, a possible range from near critical values of about 31 °C up to 200 °C reduces the amount of excess heat to be removed in the liquid cooler during high temperature runs of the rig. The baseline design was thus oriented at the upper value. Losses, also in downstream components such as diffuser and volute, which are not fully represented in the optimization, were taken into account via an assumed total-to-total efficiency of  $\eta_{tt} = 0.85$ .

The type of the impeller is further determined by the specification of two additional design variables. Accordingly, the rotational speed was set to 18000 rpm which provides a reasonable compromise between moderate speeds and practicable exit widths. Dimensionless values and the range of preferable combinations in the Cordier-diagram, finally leads to a centrifugal impeller with a diameter of approximately 72 mm and an exit width of 2.00 mm. These dimensions remained fixed for all variants during the optimization process. Subsequently, as shown in Figure 2, a full three dimensional flow path was created based on the meanline design. A three dimensional blade modeling approach as well as splitter blades were set as default. Additionally, the total number of blades were fixed to a total of 16 blades. Since only an isolated optimization

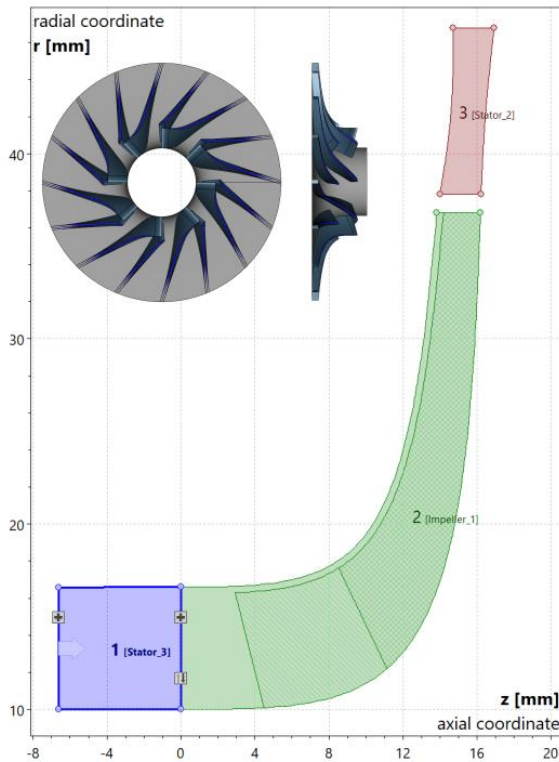


Figure 2: Meridional and component views of the baseline design.

Performance Variables			
Mass flow	$\dot{m}$	3.3	kg/s
Total inlet temperature	$T_{0,\text{tot}}$	(31) .. 200	° C
Total inlet pressure	$p_{0,\text{tot}}$	290	bar(a)
Pressure ratio	$\Pi_{\text{tot}}$	1.035	-
Estimated tot. to tot. Efficiency	$\eta_{tt}$	0.85	-
Speed	$n_{RPM}$	18000	rpm
Work coefficient	$\psi$	1.18	-
Flow coefficient	$\varphi$	0.04	-

Main Dimensions		
Hub diameter	$d_H$	20.0 mm
Suction diameter	$d_S$	33.0 mm
Impeller diameter	$d_2$	72.0 mm
Outlet width	$b_2$	2.00 mm
Tip clearance	$x_{tip}$	0.35 mm

Table 1: Performance variables and main dimensions of the baseline design.

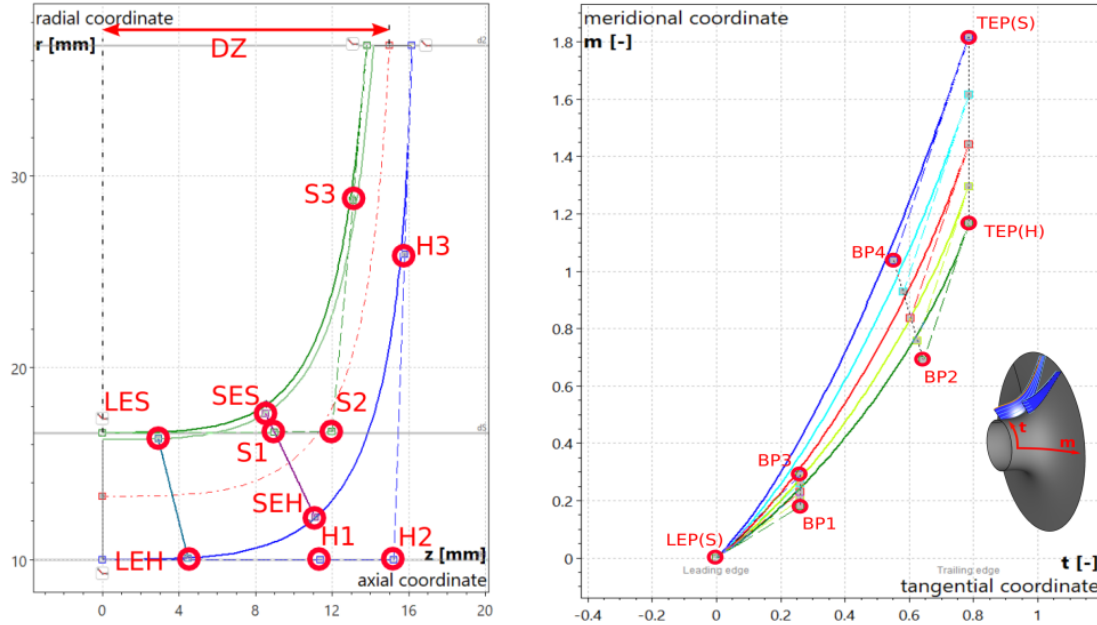


Figure 3: Design parameters of the meridional contour (left) and the blade shape (right) to vary the geometrical shape of the impeller within the optimization procedure. Please note that some points have more than one degree of freedom and therefore more than one variable.

of the impeller is carried out in this work, no detailed modifications were done for the inlet area and the diffuser. Anyway, to increase numerical stability of the CFD simulations a bladeless diffuser ring as well as a simple inflow area were added.

To allow a variation of the geometry within the optimization process, a total of 20 parameters were specified at different design levels of the impeller. The left hand side of Figure 3 shows the set of points related to the manipulation of the meridional contour. Hub and shroud are each controlled by 3 control points (H1-H3 and S1-S3, respectively), of which the second point can be changed in both axial ( $z$ ) and radial ( $r$ ) direction in each case. The beginning and end of both curves are fixed to the inlet and outlet diameters. In addition, the hub- and shroud side position of the blade leading edges can be changed in meridional direction for both main and splitter blades. A limit was set on the relative difference of both points on each blade to prevent excessive deformation. Finally, the axial extend of the impeller can be modified by  $DZ$ . In Addition to the meridional contour the blades can be modified by manipulating the Bezier curves used for modeling the blade surfaces in the conformal  $t, m$  coordinate system (tangential and meridional coordinate). Figure 3 shows a representation of the curves in the  $t$ - $m$  coordinate system containing the parameter points describing the curves. The leading and trailing blade edge position can be changed in tangential direction via the points LEP and TEP resulting in an inclination of the edges from hub to shroud. While the trailing edge can be moved on both sides, the hub and the shroud, the leading edge is fixed on the hub to provide a fixed reference. Beside that the points BP1-BP4 allow a modification of the curves shape itself and thus the blade surfaces.

Numerical evaluation was done by means of a 3D CFD model based on a single blade passage of fully hexahedral mesh by using identical mesh parameters for all input geometries. To limit the mesh size, the resolution of boundary layers was limited to  $y^+$  values below 200 resulting in an average node count of approximately 2 million nodes. To calculate the turbulence, the SST model with wall functions was used. Boundary conditions were set by applying total Temperature and pressure conditions at the inlet combined with a mass flow condition at the outlet. Walls were treated as adiabatic with no slip conditions. Additionally, a counter rotating wall velocity was set

to the shroud sided casing wall of the impeller. Rotating and static domains were connected using the frozen rotor approach. Real gas fluid properties were modeled by applying tabulated values generated from REFPROP data.

Convergence was set to a RMS residual of 1e-6 and a mass flow conservation target of 1e-3 between inlet and outlet. Only geometries giving a steady state solution by reaching this targets were treated as stable.

## EVALUATION CRITERIA AND OPTIMIZATION METHOD

As mentioned before, the impeller should be optimized for a wide operating range while satisfying the boundary conditions given by the performance variables in Table 1. Assuming the given mass flow to be the maximum and with regard to operation at lower temperatures (and thus higher densities), this means lowering the surge / stall limit of the impeller. To avoid the calculation of a complete performance line for each design, suitable criteria should be defined for rating the various geometries upon their behavior at the design point.

Within one-dimensional performance calculations, according to Aungier [4], impeller stability at lower flow rates can be evaluated using the diffusion factor as a generalized version of the Lieblein factor:

$$D_{eq} = \frac{w_{max}}{w_2} = \frac{1}{2 \cdot w_2} \cdot \left( w_1 + w_2 + \frac{2\pi \cdot d_2 \cdot u_2 \cdot I_B}{z_{eq} \cdot L_B} \right) \quad (1)$$

In which  $w_1$  and  $w_2$  respectively stand for the relative velocity at the entrance and the exit of the impeller (bladed section).  $w_{max}$  denotes the maximum relative velocity over the flow path and  $u_2$  the peripheral speed at the impeller outlet. As geometric values  $d_2$  is the impeller diameter while  $z_{eq}$  is an equivalent number of blades and  $L_B$  the blade length. Finally,  $I_B$  is the blade work input coefficient which evaluates to:

$$I_B = \frac{c_{u2}}{u_2} - u_1 \cdot \frac{c_{u1}}{u_2^2} \quad (2)$$

Therein  $c_{u1}$  and  $c_{u2}$  denote the corresponding circumferential component of the absolute velocity at the inlet and outlet.  $u_1$  and  $u_2$  denote the respective circumferential velocity. Impeller stall can be assumed when  $D_{eq}$  exceeds a value of 2. Applied within one dimensional calculations of performance curves by Klausner and Gampe [5] this criteria resulted in good agreement with experimental data for several impellers. On this base, the simplified assumption was made that, at the same operating point, impellers with a small diffusion factor cover a wider operating range than those with large diffusion factors. This results in the minimum possible diffusion factor as the first optimization target. However, as can be seen from Equation (1) a low diffusion factor is a tradeoff of higher values for  $w_2$  and the energy input to the fluid represented by the blade work input coefficient  $I_B$ . To limit the tendency for low diffusion factors to be achieved by comparatively high values for  $w_2$ , low relative outflow velocities are set as secondary optimization goal. In Addition to that, a minimum pressure difference of  $\Pi_{tot} = 1.036$  was set as an additional condition to be fulfilled by favorable designs during the optimization process, avoiding a violation of the boundary conditions specified in Table 1. Finally, the full optimization target reads:

$$\min(D_{eq}) \wedge \min(w_2) \mid \pi_{tot} \geq 1.036 \quad (3)$$

For optimization a multi-objective genetic algorithm (MOGA) was used within the software toolkit Dakota [6], provided by the Sandia National Laboratories. The algorithm imitates evolutionary

principles by using the best design points from a population to form subsequent generations. In contrast to gradient-based optimization methods, this method searches for a global optimum within the given constraints. The size of the initial population was set to 300 individuals, with geometry generated by random variable variation. Subsequent population sizes were set automatically by the algorithm within a similar size.

## RESULTS AND DISCUSSION

Optimization was done by evaluating a total 1067 designs within four populations. As a result overview, Figure 4 shows the evolution of  $D_{eq}$  over four generations. Looking at the fraction of valid designs, it can be seen that the automated combination of the design variables did not result in a valid impeller geometry in about 10-15% of the cases. This persists also in later evolutions, which shows that even the combination of favorable designs by the algorithm can result in new faulty geometries. Nevertheless, the increase in the fraction of feasible solutions, defined as these which fulfill all target criteria, shows a trend to better designs with each generation. Compared to the initial population, this value has almost doubled within the last stage. In the same context, as indicated at the bottom of the plot, mean values for  $D_{eq}$  could be successfully lowered within each new population. Additionally, an visible increase in the amount of grayed out (not converged) solutions for higher values of  $D_{eq}$  confirms its relation to the stability of the operating point. Looking at lower values for  $D_{eq}$ , the previously mentioned influence of the work input coefficient  $I_B$  (cf. Equation (2)) is noticeable. As can be seen by the solutions crossed out in Figure 4, most of the designs resulting in a value of  $D_{eq} < 1.6$  did not reach the minimum pressure ratio set by the boundary conditions given in Table 1.

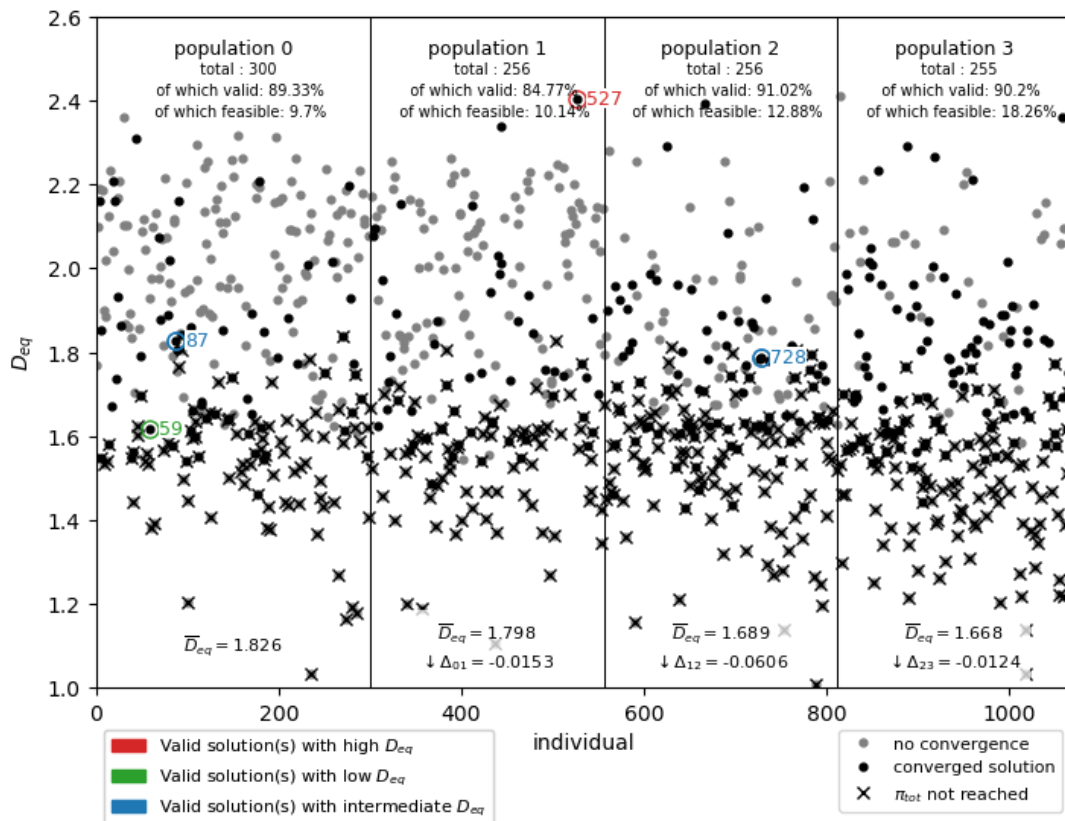


Figure 4: Result overview of the optimization with highlighting of individual designs.

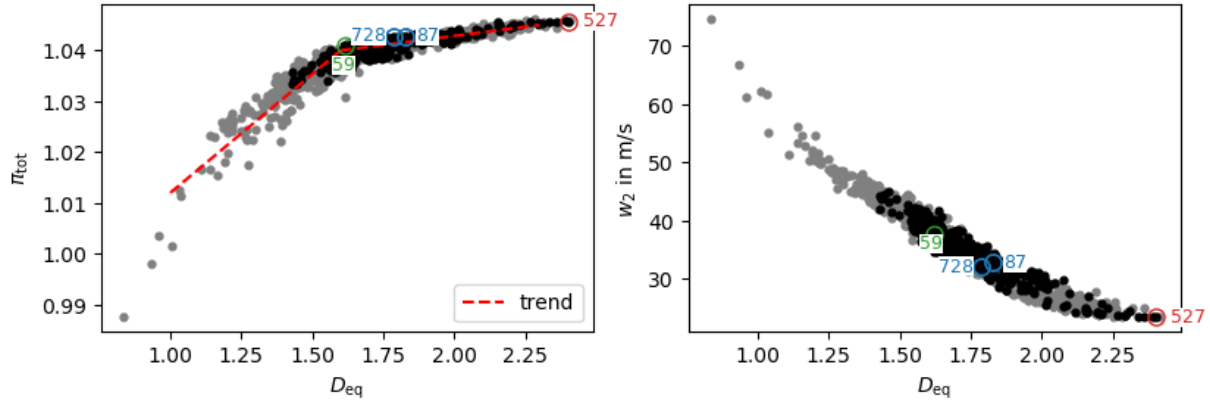


Figure 5: Comparison of the equivalent diffusion factor against the pressure ratio (left) and the impellers relative exit velocity (right).

Figure 5 compares the equivalent diffusion factor  $D_{eq}$  of the individual designs with the pressure ratio  $\Pi_{tot}$  and the impellers relative outflow velocity  $w_2$ . Due to the previously described conflicting dependence of this three variables on each other, the formation of a Pareto front can be seen in both plots. The selection of a suitable design is therefore a matter of weighing up the individual values against each other. Within this context, two lines have been plotted in the left graph reflecting the tendency of  $\Pi_{tot}$  to change with increasing  $D_{eq}$ . From the intersection of both lines, only relatively small increases in the pressure ratio are achieved with larger values for the diffusion factor. Consequently, it can be assumed that designs in this region provide a good compromise between low equivalent diffusion factors and a high pressure differences. To make a more detailed comparison of several designs by considering also the relative outflow velocity  $w_2$ , a total of four impeller designs were selected by means of the following criteria. One design representing the solution with the highest pressure ratio in a range of 5% around the intersection point of both trend lines at  $D_{eq}=1.60$ . Two designs representing the highest possible pressure difference within values for  $D_{eq}$  in a range of 1.60 to 1.80. And finally, one design representing a valid solution with the highest value for  $D_{eq}$  over all designs. All selected designs are highlighted with a green, blue or red marker in Figure 4 and Figure 5 according to the respective criterion.

Beginning with design number 59, the right plot in Figure 5 shows that the low values for  $D_{eq}$  are achieved with comparatively high values of approx. 38 m/s for  $w_2$ . In contrast, the design with the highest diffusion factor, represented by individual number 527, as expected shows the lowest relative exit velocities of about 24 m/s. It is also remarkable that despite an equivalent diffusion factor clearly above the aforementioned critical value of 2.00, a stable solution could be achieved. Taking into account the two intermediate designs, highlighted in blue and given by the numbers 87 and 728, it can be seen that, compared with design number 59, significantly lower exit velocities are achieved. Despite nearly identical values for  $\Pi_{tot}$  of both designs, individual 728 reaches a noticeably lower diffusion factor as well as lower relative outflow velocities.

Figure 6 shows a comparison of performance lines for all four designs, including the evolution of  $D_{eq}$  and  $w_2$  with changing mass flows as well a front and a side view of each geometry. As expected from the relation of the diffusion factor to the blade length shown in Equation (1), the visible differences in the impeller geometry show a tendency to a larger axial extension as well as to longer splitter blades with higher diffusion factors. Additionally, a more pronounced rake angle of the blade can be seen at higher values for  $D_{eq}$ . Comparing the pressure ratio against the relative mass flow in the uppermost plot, all four designs provide a negative slope of the pressure rise curve with fairly similar gradients. In contrast, the middle subplot shows a different behavior for the equivalent diffusion factors which for the compared geometries forms a steeper

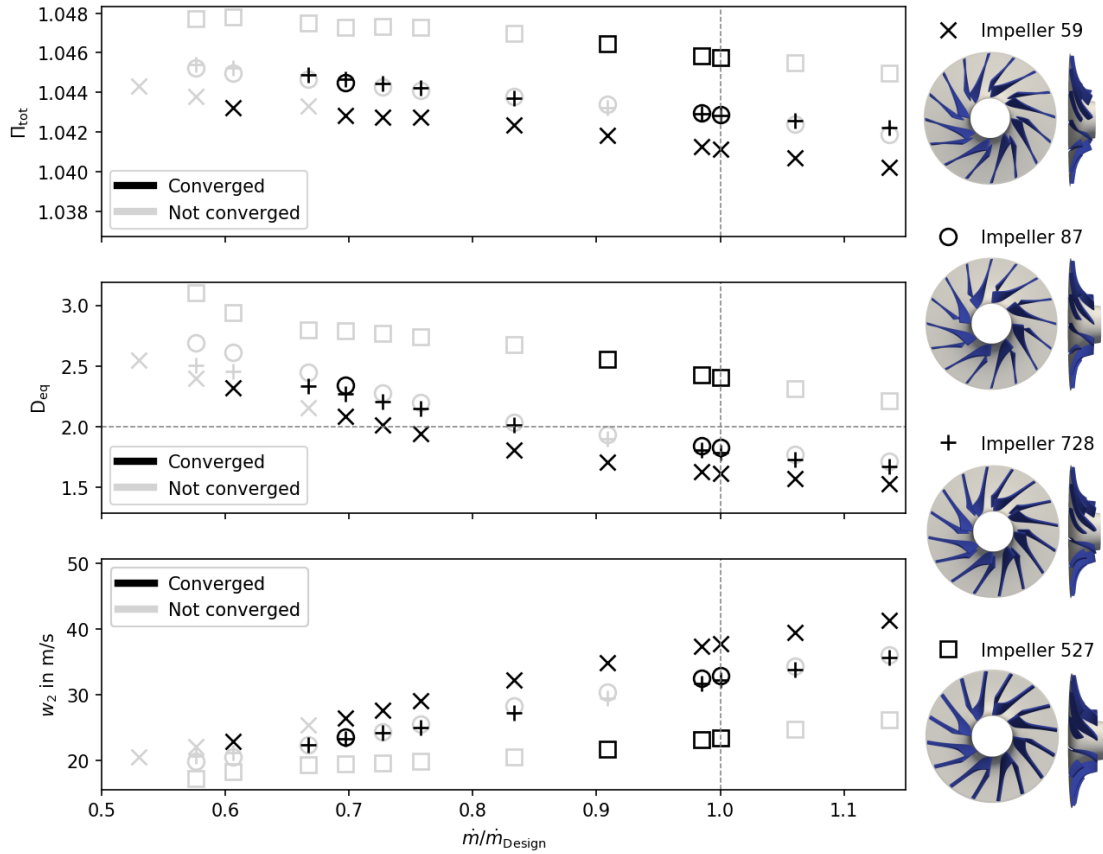


Figure 6: Performance lines of selected designs compared to the evolution of equivalent diffusion factor and relative impeller outlet velocity with changing mass flows.

slope for low diffusive designs. Considering the relative exit velocities in the subplot at the bottom of Figure 6 this trend is almost reversed, indicating the previously described relation between the two variables.

Regarding the stability limits, the number of non-converged solutions, indicated by the grayed out markers, it can be seen that the designs with a lower  $D_{eq}$  show stable points down to lower mass flows. Whereas impeller number 527, the design with the highest  $D_{eq}$ , reveals only a limited range down to relative mass flows of 0.9. In contrast, impeller number 59, the design with the lowest value for  $D_{eq}$ , has stable solutions down to values of approx. 0.6. By comparing the two intermediate designs, a distinct similarity between the performance lines can be seen. Similarly, there are only minor visible differences in the geometries of both impellers, shown on the right side of Figure 6. Most noticeable aspects are a slightly more pronounced rake of the blades as well as a higher length of the splitter blades in design 728. However, significant differences in the stability are noticeable. While design 728 shows up an almost continuous stable operation in a mass flow range for relative values between 0.675 and 1.15, impeller 87 shows only three stable points including a large gap between two points near design conditions and the lowest stable value. This shows that the diffusion factor is a good indicator but not a guarantee for a wide operating range.

Finally, design 728 was selected as the preferred variant. On this base, like shown in Figure 7, a solid model was created to be further used in stress analyses. On the fluid side a full stage design was completed by adding a vaneless diffusor and a volute to also provide a base for full stage range analyses and casing design.

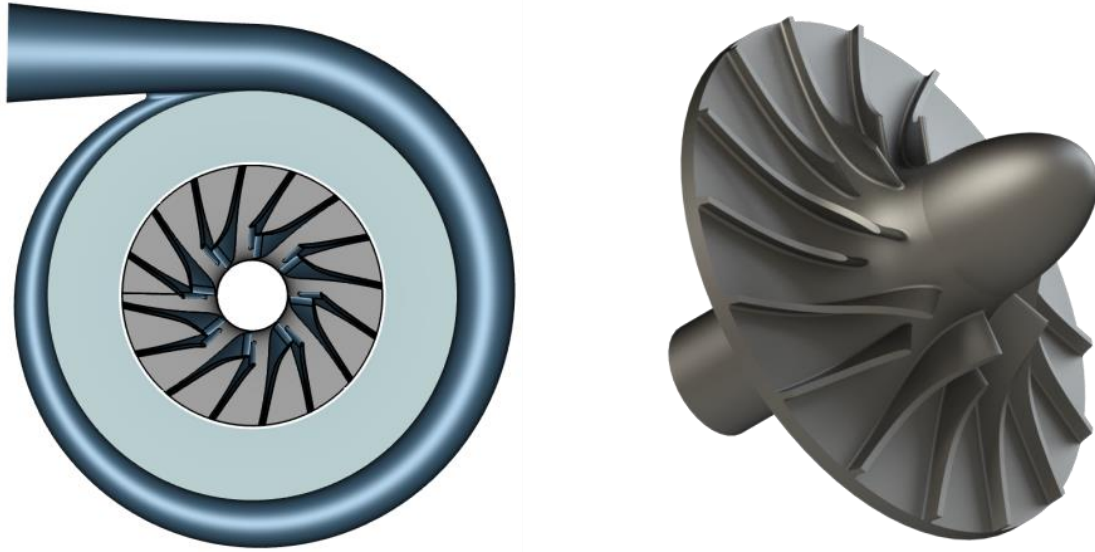


Figure 7: Preliminary stage design and solid impeller model based on the optimized geometry

## CONCLUSION

Within the CARBOSOLA project, a large scale experimental test rig is being set up by scientific and industrial partners to actively contribute to the development of sCO<sub>2</sub> technology. Since the first expansion stage does not include an expansion device, fluid circulation should be provided by a centrifugal compressor with a low pressure ratio and a preferably wide operating range, to provide a high degree of flexibility. In this context, the numerical optimization of the impeller was carried out within this work.

Starting from a baseline geometry a total of 1067 designs were created and evaluated numerically. To limit the computational effort, the equivalent diffusion factor, taken from one-dimensional performance analysis theory, was used as a criterion to estimate the operating range of each design. Additionally, conditions for the pressure ratio and the outflow velocities were applied to avoid improper optimization or violations of the boundary conditions. From the optimization results performance lines for 4 different designs were calculated and compared against each other.

The results have shown, that the diffusion factor can be used as a suitable optimization target to obtain a wide operating range. However, it could also be shown, that a low diffusion factor can be an indication but not a guarantee of a wide operating range, which is in accordance with the literature stating multiple influences on the operating range [4], [7]. Finally, a preferred impeller variant was selected and completed to a preliminary compressor design by adding a vaneless diffuser and a volute. On this basis, further design steps will be carried out in future works, including additional inflow conditions, the solid design and the casing structure.

## REFERENCES

- [1] S. Ibaraki and I. Tomita, "Optimized design and flow physics of a wide operating range centrifugal compressor for automotive turbochargers," p. 16.
- [2] M. Yagi, T. Kishibe, T. Shibata, H. Nishida, and H. Kobayashi, "Performance Improvement of Centrifugal Compressor Impellers by Optimizing Blade-Loading Distribution," in *Volume 6: Turbomachinery, Parts A, B, and C*, Berlin, Germany, Jan. 2008, pp. 1639–1648. doi:

10.1115/GT2008-51025.

- [3] R. Pelton, S. Jung, T. Allison, and N. Smith, "Design of a Wide-Range Centrifugal Compressor Stage for Supercritical CO<sub>2</sub> Power Cycles," in *Proceedings of ASME Turbo Expo 2017*, Charlotte, NC, USA, 2017, vol. GT2017, p. 8.
- [4] R. H. Aungier, *Centrifugal Compressors - A Strategy for Aerodynamic Design and Analysis*, 1st ed. New York: ASME Press, 2000.
- [5] E. Klausner and U. Gampe, "Evaluation and Enhancement of an One-Dimensional Performance Analysis Method for Centrifugal Compressors," *GT2014-25141*, vol. Proceedings of ASME Turbo Expo 2014, p. 11, 2014.
- [6] B. M. Adams *et al.*, "Dakota, A Multilevel Parallel Object-Oriented Framework for Design Optimization, Parameter Estimation, Uncertainty Quantification, and Sensitivity Analysis: Version 6.13 User's Manual," Sandia National Laboratories, Sandia Technical Report SAND2020-12495, 2020.
- [7] R. Van den Braembussche, *Design and Analysis of Centrifugal Compressors*, 1st ed. ASME Press and John Wiley & Sons Ltd, 2019.

## ACKNOWLEDGEMENTS

This work has been carried out within the project CARBOSOLA funded by the German Federal Ministry for Economic Affairs and Energy, grant reference: 03EE5001B. The authors would like to express their gratitude for the financial support of this project. The authors alone are responsible for the content of this paper.

Gefördert durch:



aufgrund eines Beschlusses  
des Deutschen Bundestages